

Role of Electrotonic Current in Excitable Cells



Emilio Macchi, Ezio Musso, and Stefano Rossi

Abstract The aim of the present chapter is to review basic properties of electrotonic current flow in excitable cells, such as neuronal axons and cardiac tissue, during subthreshold stimulation, excitation threshold and impulse conduction. Electrotonic current is proportional to the spatial gradient of the transmembrane potential and consists of a current flow across the membrane with the effect to depolarize it. There is a close interrelationship between electrotonic current that originates from local source-sink interactions and excitation threshold. Successful impulse conduction requires that the amount of active current supplied by the membrane at the source location must be equal to or exceed the amount of electrotonic current required to excite the membrane at the sink location. Such condition is determined by the state of membrane excitability at the source, at the sink and by the degree of electrical coupling between source and sink. Conversely, conduction slowing induced by source-sink mismatch in cardiac tissue may be responsible for unidirectional conduction block and reentry, a condition leading to increased arrhythmia vulnerability, both in normal and pathological tissue. In addition to affecting impulse conduction, electrotonic current flow originating from an activation sequence locally modulates action potential repolarization, determining its duration and spatial dispersion across the tissue. Ultimately, experimental evidence is presented in support of the hypothesis of electrotonic current modulation of ventricular repolarization by two different activation sequences, sinus beat and ventricular test site drive, in normal rat heart.

E. Macchi (✉) · E. Musso
Dipartimento di Scienze Chimiche, della Vita e della Sostenibilità Ambientale, Università di Parma, Parma, Italy
e-mail: emilio.macchi@unipr.it

S. Rossi
Dipartimento di Medicina e Chirurgia, Università di Parma, Parma, Italy

© Springer Nature Switzerland AG 2018
D. Boffi et al. (eds.), *Mathematical and Numerical Modeling of the Cardiovascular System and Applications*, SEMA SIMAI Springer Series 16,
https://doi.org/10.1007/978-3-319-96649-6_5

87

1 Introduction

Considerable data has been reported concerning the spread of electrotonic current in excitable cells such as along neuronal axons and between neighboring cells in cardiac muscle. Electrotonic current is proportional to the membrane potential difference between neighboring cells and consists of a current flow across a membrane with the effect to depolarize its membrane potential. However, an accurate definition and description of electrotonic current, an important prerequisite for understanding the mechanisms of impulse initiation and conduction in excitable cells, is not readily available in the literature. In addition, experience gathered in teaching electrophysiology to Biology students suggests that, although the common significance of electrotonic current may be readily understood, still its intimate mechanism is not easily grasped. Indeed, the close relationship between electrotonic current and threshold of excitation is usually ignored in electrophysiology textbooks. Electrotonic current originates from local source-sink interactions that determine conduction of excitation in cardiac tissue. Successful propagation requires that the amount of active current supplied by the membrane at the source location must be equal to or exceed the amount of electrotonic current required to excite the membrane at the sink location. At the cellular level, this condition is determined by the state of membrane excitability at the source and the sink and by the degree of electrical coupling between source and sink. At the macroscopic scale of multicellular tissue, this condition is strongly influenced by structural properties of myocardium, such as branching of fibers or heterogeneities of electrical coupling over tissue segments. Moreover, the relevance of electrotonic current in sustaining impulse conduction extends beyond normal propagation. Over the last decades electrotonic current mismatch has been increasingly recognized as a potential substrate for abnormal rhythms and reentry, both in normal as well as pathological conditions. For example, electrotonic conduction slowing may be responsible for unidirectional conduction block and reentry, a condition leading to increased myocardial *arrhythmia vulnerability*.

In addition to affecting action potential conduction, electrotonic current modulates action potential repolarization determining its duration and spatial variation (dispersion) across the tissue. The influence of electrotonic current on the repolarization phase of a propagating action potential is commonly undervalued in spite of the relevance of electrotonic modulation by the activation sequence.

Hence, the present chapter aims to review basic properties of electrotonic current flow in excitable cells during subthreshold and threshold stimulation and during action potential conduction. We also present some experimental evidence that supports the hypothesis of electrotonic current modulation of repolarization.

2 Linear Cable Model of Excitable Cells

The linear cable, as equivalent model of excitable cells (see, e.g. [1]), represents transmembrane current i_m as the sum of two components, the capacitive (or displacement) current i_c and the ionic (or resistive) current i_{ion} (Fig. 1). Within excitable cells, current is carried by ions, primarily sodium, potassium, chloride and calcium.

Capacitive current i_c is a displacement of ionic charges on either side of cell membrane without movement across the membrane. For an ion deposition on one side of the membrane, an ion withdrawal of the same sign occurs on the opposite side. Capacitive current is much more important than one might at first suspect, because cell membrane is very thin and thus highly capacitive.

Conversely, ionic current i_{ion} consists of ions that physically cross membrane ion channels.

In brief, $i_m = i_c + i_{ion}$ with i_m , i_c , i_{ion} currents per unit length of the cell.

By definition, capacitive current $i_c = c_m \frac{\partial V_m}{\partial t}$, with c_m membrane capacitance per unit length of the cell, $V_m = V_i - V_e$ membrane potential and V_i , V_e intracellular and extracellular potential, respectively. Ionic current i_{ion} is *resistive*, i.e. according to Ohm's law, through passive ion channels, and *active* through voltage-gated, ligand-gated or mechanosensitive ion channels.

The change in potential per unit length along the intracellular (or extracellular) axial path equals the axial current times the intracellular (or extracellular) resistance/unit length (i.e., a voltage drop according to Ohm's law).

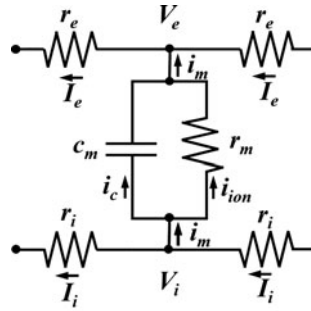


Fig. 1 Electrical equivalent circuit of the linear cable model of excitable cells. Parallel resistance r_m and capacitance c_m represent cell membrane impedance with corresponding i_{ion} and i_c current flow, respectively. Transmembrane current i_m is given by $i_m = i_{ion} + i_c$. I_i . Longitudinal extracellular and intracellular currents are I_e and I_i , extracellular and intracellular potentials are V_e and V_i and extracellular and intracellular resistances per unit length are r_e and r_i , respectively. Current flow is due to subthreshold point stimulation from an intracellular anode outside the right side of the circuit or an extracellular cathode outside the left side of the circuit

Consequently,

$$I_i = -\frac{1}{r_i} \frac{\partial V_i}{\partial x} \quad \text{and} \quad I_e = -\frac{1}{r_e} \frac{\partial V_e}{\partial x},$$

with I_i , I_e intracellular and extracellular axial current, r_i , r_e intracellular and extracellular axial resistance per unit length, respectively and the axial variable is x . The minus signs arises because we define positive longitudinal currents to be flowing in the positive x direction. The potential must *decrease* with *increasing* x for current to flow in the positive x direction because current flows from higher to lower potential values.

If a portion of intracellular axial current I_i leaves the intracellular space by outward crossing the membrane, then the axial decrease is transformed into a transmembrane current i_m and extracellular axial current I_e increases. The changes in axial current per unit length must precisely equal the transmembrane current per unit length, because the total current must be conserved, i.e.:

$$i_m = -\frac{\partial I_i}{\partial x} = \frac{\partial I_e}{\partial x}.$$

By definition, transmembrane current i_m is considered to have a positive sign when it flows across the membrane in the direction from the inside to the outside.

Hence, from the previous definitions we have:

$$i_m = \frac{1}{r_i + r_e} \frac{\partial^2 V_m}{\partial x^2}.$$

In fact, by deriving twice both members of $V_m = V_i - V_e$, we obtain at first:

$$\frac{\partial V_m}{\partial x} = \frac{\partial V_i}{\partial x} - \frac{\partial V_e}{\partial x} = -r_i I_i + r_e I_e,$$

and then:

$$\frac{\partial^2 V_m}{\partial x^2} = -r_i \frac{\partial I_i}{\partial x} + r_e \frac{\partial I_e}{\partial x} = r_i i_m + r_e i_m = (r_i + r_e) i_m.$$

The extracellular axial current may increase with axial distance x either due to the arrival of current that crosses the membrane (transmembrane current, i_m) or the introduction of a stimulus current from outside the preparation through inserted electrodes. In presence of impressed current, i.e. extracellular, $\frac{\partial I_e}{\partial x} = i_m + i_s$, where i_s the impressed current per unit length, positive for current entering the extracellular space via *polarizing* electrodes. The units for i_s then correspond to the same units

used for i_m . In this case, it results:

$$\frac{\partial^2 V_m}{\partial x^2} = (r_i + r_e) i_m + r_e i_s.$$

Thus, when $i_s = 0$, i_m is directly proportional to $\frac{\partial^2 V_m}{\partial x^2}$ and depends only on r_i and r_e .

2.1 Units of Resistance and Capacitance

If r is the resistance (ohm) of a box of conducting material of length L (cm) and section area A (cm²) through which ionic current flows, then $r = R \cdot L/A$, where R (ohm-cm) is the resistivity of the conducting material. The resistivity is defined as the resistance of a unit box of conducting material ($L = 1$ cm, $A = 1$ cm²).

Hence, units of intracellular/extracellular resistance per unit length, i.e. $r_{i,e} = r/L = R_{i,e}/A$, are ohm/cm where $R_{i,e}$ is the intracellular/extracellular resistivity, respectively.

Units of membrane resistance per unit/length r_m are defined by considering a thin sheet of resistive material instead of the conducting box, with thickness l infinitesimal (δl). Hence, membrane resistivity $R_m = R \cdot \delta l$ has units ohm-cm². By considering the surface area A (cm²) of a length of cell membrane L (cm), i.e. $A = s \cdot L$ with s (cm) the cell circumference, then membrane resistance per unit length is defined by $r_m = r \cdot L = R_m/s$ in units ohm-cm.

If c is the capacitance (microfarad) of a cell membrane of length L (cm), circumference s (cm) and area $A = L \cdot s$ (cm²) through which capacitive current flows, then $c = C_m \cdot A$ where C_m (microfarad/cm²) is the membrane capacity, defined as membrane capacitance per unit area. Accordingly, membrane capacitance per unit length is defined as $c_m = c/L = C_m \cdot s$ in units microfarad/cm.

3 Electrotonic Current and Potential

An extracellular point *current source* of strength i_s , such as a point electrode connected with the positive or negative pole of an external current generator, positioned close to an excitable cell, generates an extracellular current I_e that flows away from the positive pole (Fig. 2a, upper panel) or toward the negative pole (Fig. 2a, lower panel), respectively. A fraction of extracellular current I_e crosses cell membrane as transmembrane current i_m that transforms into intracellular current I_i flowing along the cell axis x . At steady-state, a potential gradient $\Delta V_m(x)$ exists along the cell axis where i_m crosses the membrane. Transmembrane current i_m is the *electrotonic current* and the membrane potential gradient $\Delta V_m(x)$ generated by i_m

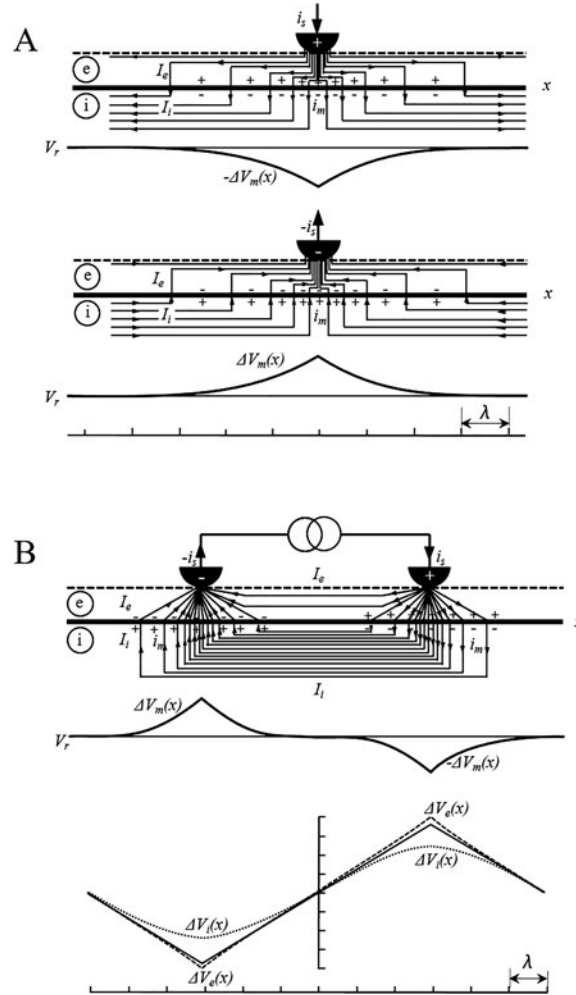
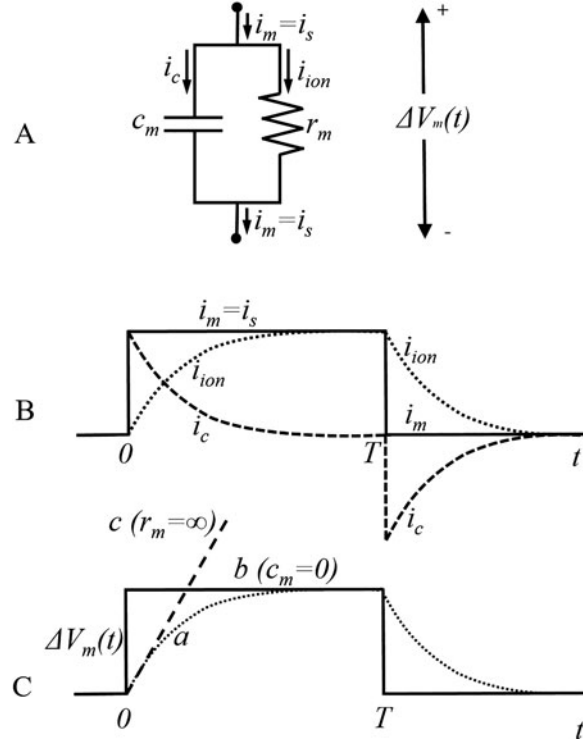


Fig. 2 Schematic diagrams showing steady-state current flow during extracellular stimulation from a current generator of i_s strength. **(a)** Upper panel: unipolar anodal stimulation. Lower panel: unipolar cathodal stimulation. **(b)** Upper panel, bipolar stimulation. Lower panel: theoretical voltage changes following bipolar stimulation; the straight line represents ΔV_e and ΔV_i , extracellular and intracellular voltage changes, respectively, at the make of the stimulus; the dashed and dotted lines represent steady-state values of ΔV_e and ΔV_i , respectively. In each diagram: x , longitudinal distance; λ , space constant; e and i , extracellular and intracellular space, respectively; thick horizontal line, cell membrane; dashed horizontal line, surface of extracellular conducting layer; arrowed straight lines, extracellular (I_e), intracellular (I_i) and transmembrane (i_m) current lines, respectively where density of current lines is not directly proportional to current field density; $\Delta V_m = \Delta V_i - \Delta V_e$, transmembrane voltage change; V_r , resting potential

Fig. 3 (a) parallel resistance (r_m) and capacitance (c_m) circuit representing cell membrane impedance. (b) Time change of transmembrane current i_m , capacitive current i_c and ionic current i_{ion} , during and following application to the circuit shown in A of a step current pulse of strength i_s and duration T. (c) Time change of transmembrane voltage $\Delta V_m(t)$ for: (a) parallel r_m and c_m circuit; (b) purely r_m circuit; (c) purely c_m circuit, respectively, during and following application of a step current pulse of strength i_s and duration T



along the cell axis is the *electrotonic potential*. The amplitude of the electrotonic potential is highest at the source location and decreases exponentially with the distance away from the source proportionally to i_m . At distance of a few space constants λ ($\lambda = \sqrt{\frac{r_m}{r_i + r_e}}$) from the source, $i_m = 0$ so that also $\Delta V_m = 0$ and V_m is spatially constant at its resting potential V_f [1].

By representing a membrane segment δx , small enough that the transmembrane voltage is the same all across the patch, with the electrical equivalent circuit of Fig. 3a, the electrotonic current i_m that flows across the membrane is given by $i_m = i_c + i_{ion}$. Capacitive current i_c adds or subtracts positive charges on one side of the membrane and an equivalent number of negative charges on the other side and the charge change of the membrane capacitor generates the membrane potential change $\Delta V_m(t)$ that causes ionic resistive current i_{ion} to flow.

In summary, the membrane capacitor is charged or discharged by capacitive current i_c . The charge change in time on the capacitor creates membrane potential change $\Delta V_m(t)$ that generates ionic resistive current i_{ion} to flow through r_m with the same orientation of i_c . Membrane resistance per unit length r_m is passive when voltage dependent ion channels are at their resting state. In presence of a rectangular current pulse of subthreshold strength, the electrotonic potential $\Delta V_m(t)$ is an exponential function of time with time constant $\tau = r_m c_m$ (subthreshold

response) (Fig. 3c, line *a*) and $i_{ion}(t) = \Delta V_m(t)/r_m$ is also an exponential function with the same time constant (Fig. 3b) (see [1]). Ionic current i_{ion} is resistive when membrane resistance per unit length r_m is passive, i.e. below activation threshold of voltage dependent channels, and does not affect the charge on the membrane surface. Thus, near the extracellular current source, transmembrane current i_m is given by $i_m = i_c + i_{ion}$: capacitive component i_c generates the electrotonic potential, and resistive ionic component i_{ion} is generated by the electrotonic potential with both i_c and i_{ion} flowing in the same direction and orientation.

Particularly, outward electrotonic current i_m depolarizes the membrane by adding positive charges by means of i_c on the inside of membrane surface, while inward electrotonic current i_m hyperpolarizes the membrane by adding positive charges by means of i_c on the outside of membrane surface (Fig. 2). In both cases, resistive ionic current i_{ion} is represented by positive ions crossing the membrane with the same direction and orientation of the capacitive current without affecting the charge on the two sides of the membrane. Hence, in the region of outward i_m , it is not outward i_{ion} that depolarizes the cell. The situation is rather the other way round: an outward ionic current i_{ion} flows because the cell is depolarized by the capacitive current i_c . In fact, a step current pulse generates an electrotonic potential ΔV_m even if membrane resistance was infinite (Fig. 3c, line *c*). The transmembrane current would then be entirely capacitive and the change in membrane potential would be simply proportional to the amount of charge applied, i.e. $\Delta V_m(t)$ would change linearly with time due to the charge accumulating on the two sides of the membrane. In case of a purely resistive circuit ($c_m = 0$), $\Delta V_m(t)$ changes simultaneously as the step current pulse (Fig. 3c, line *b*).

In excitable cells, electrotonic current can be generated by:

- (a) current injection from an electrode connected with a current generator;
- (b) membrane electromotive force (i.e. propagating action potential) generating *active* transmembrane ionic current i_{ion} .

4 Subthreshold Stimulation

Current injection is extracellular if both electrodes connected with the current generator are external to the cell (Fig. 2), while it is intracellular if one of the two electrodes is positioned inside the cell (Fig. 3a, electrical equivalent circuit). Furthermore, extracellular current injection is unipolar if the return current electrode is located at great distance from the current injection electrode (Fig. 2a), or bipolar if both electrodes are next to each other (Fig. 2b).

4.1 Intracellular Current Injection

In this setting, the intracellular microelectrode is connected to an anode (positive pole) or a cathode (negative pole), while the return current electrode is extracellular. In presence of an intracellular anode the current flows outward from the cell depolarizing the membrane, while in presence of an intracellular cathode the current flows into the cell hyperpolarizing the membrane. If the extracellular electrode is close to the microelectrode in the stimulated cell, current lines are mostly comprised within the inter-electrode region, while if the extracellular electrode is at a great distance, current lines display radial flow from the intracellular electrode.

Let us consider an intracellular rectangular current injection of subthreshold strength i_s , as occurs in an isolated cell or a uniformly polarized cardiac Purkinje fibre [2]. The electrical equivalent circuit is represented in Fig. 3a. At $t = 0$, current pulse onset, $i_c = i_s$ while $i_{ion} = 0$ (Fig. 3b). Subsequently, i_c decreases exponentially toward zero with time constant τ (Fig. 3b, $0 < t < T$). The charging of the capacitor generates an exponential potential change $\Delta V_m(t)$ (Fig. 3c, line a , $0 < t < T$) and a corresponding exponential increase in i_{ion} toward steady-state i_s (Fig. 3b, $0 < t < T$). During the current pulse, both i_c and i_{ion} flow across the membrane with the same orientation and satisfy at each instant the relationship $i_m = i_s = i_c + i_{ion}$. Under steady-state conditions, i_m is simply represented by its resistive component $i_{ion} = i_s$ since $i_c = 0$ (Fig. 3b, $0 < t < T$). At $t = T$, current pulse offset, $i_m = i_c + i_{ion} = 0$ and $i_c = -i_{ion}$, i.e. i_c and i_{ion} flow across the membrane with opposite orientation (Fig. 3b, $t > T$), discharging the capacitor c_m through the resistor r_m while the potential decreases exponentially toward zero (Fig. 3c, line a , $t > T$).

4.2 Extracellular Current Injection

Extracellular current injection is unipolar when one electrode, anode or cathode, is close to the cell membrane and the other electrode is at infinite distance (Fig. 2a) while it is bipolar when both electrodes, anode and cathode, are in close proximity to the cell membrane at short inter-electrode distance (Fig. 2b). Due to the higher resistance of the membrane compared to extracellular resistance, a small fraction of the injected current from an electrode crosses the membrane as electrotonic current i_m flowing along cell axis as intracellular current I_i , while the larger fraction of the injected current flows as extracellular current I_e . Electrotonic current i_m is inward at the anode and hyperpolarizes the membrane along a distance of few λ (Fig. 2a, upper panel). Electrotonic current i_m is outward at the cathode and depolarizes the membrane along a distance of few λ (Fig. 2a, lower panel). Beyond a distance of a few λ from the poles, electrotonic current $i_m = 0$ and electrotonic potential $\Delta V_m = \Delta(V_i - V_e) = \Delta V_i - \Delta V_e = 0$. In fact, beyond a distance of a few λ from the poles, ΔV_i and ΔV_e change linearly along cell axis according to Ohm's law because I_i and I_e are constant and $\Delta V_i = r_i \cdot I_i$ and $\Delta V_e = r_e \cdot I_e$ have the same amplitude

and sign [3]. For bipolar current injection, Fig. 2b, lower panel, represents steady-state voltage changes ΔV_i (dotted line) and ΔV_e (dashed line) and instantaneous voltage changes at the make of the stimulus ΔV_i and ΔV_e (straight line). In case of anodal and cathodal unipolar current injection, intracellular and extracellular currents flow from the anode to infinity (Fig. 2a, upper panel) and toward the cathode from infinity (Fig. 2a, lower panel), respectively. In case of bipolar current injection both intracellular and extracellular currents flow from anode to cathode within the inter-electrode distance (Fig. 2b, upper panel).

Detailed analytical solution for the temporo-spatial response of an infinite cable to a current step is described, for example, in Jack et al. [4] and Plonsey and Barr [1].

5 Stimulation Threshold

When an excitable membrane reaches excitation threshold, it becomes itself a membrane current source or a local membrane electromotive force and, as such, can elicit a “*membrane action potential*” in absence of electrotonic current ($i_m = 0$) or a “*propagating action potential*” in presence of electrotonic current ($i_m \neq 0$). Requirements for reaching excitation threshold for the two conditions are different.

5.1 The Membrane Action Potential

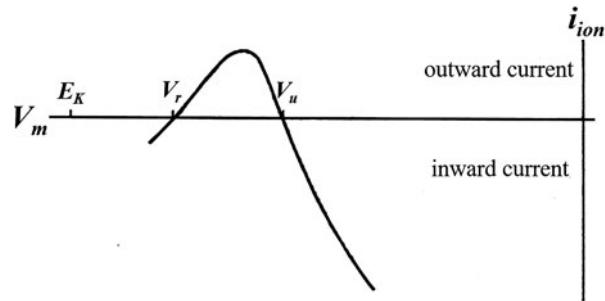
Let us consider the case of a cell in which the whole membrane surface experiences the same potential changes at the same time, i.e. the membrane is clamped spatially, and there is no intracellular current flowing along cell axis. This condition occurs in an isolated cardiomyocyte, in shortened segments of Purkinje fibers or in a squid giant axon by the use of an internal silver wire which makes the squid axon membrane isopotential [2, 5]. In this setting, the membrane will become a current source when membrane potential V_m is depolarized from resting potential V_r to a threshold potential V_u (*uniform threshold potential*).

In a squid giant axon, not considering pumps and exchangers and in absence of the inward rectifier current I_{KI} , resting potential V_r is characterized by net ionic transmembrane current $i_{ion} = 0$ (electrical equilibrium) as the result of opposite ion diffusions, mainly through Na^+ and K^+ passive ion channels, respectively. In this setting,

$$i_{ion} = i_{Na} + i_K = (V_r - E_{Na}) \cdot g_{Na} + (V_r - E_K) \cdot g_K = 0,$$

with E_{Na} , E_K equilibrium potential, and g_{Na} , g_K membrane conductance for Na^+ and K^+ , respectively. Extracellular cathodal current injection modifies resting potential V_r , by depolarizing V_m towards more positive values (Fig. 4). At the

Fig. 4 Steady-state membrane current/voltage (i_{ion}/V_m) relation defining voltage threshold V_u for cable excitation by uniform polarization. E_K , K^+ equilibrium potential; V_r , resting potential



beginning of depolarization, while g_{Na} and g_K remain constant, outward K^+ current i_K increases because $V_m - E_K$ increases and inward Na^+ current i_{Na} decreases because $V_m - E_{Na}$ decreases and, as a consequence, net ionic current i_{ion} becomes outward (Fig. 4). However, when the increase in depolarization activates voltage dependent Na^+ channels, inward i_{Na} current increases due g_{Na} increase and net outward ionic current i_{ion} , after reaching a maximum, gradually decreases. With a further increase in depolarization, outward net ionic current i_{ion} becomes zero again at potential $V_m = V_u$. While V_r is a steady-state electrical equilibrium, V_u represents a highly unstable electrical equilibrium due to the counterbalance of high strength inward and outward currents through low resistance active ion channels. Electrical equilibrium instability is manifested by the i_{ion}/V_m relationship displaying negative slope (conductance) at V_u compared to positive slope at V_r (Fig. 4). Hence, if current injection is terminated at $V_m = V_u$, a small spontaneous depolarization will initiate an action potential simultaneously on every patch of membrane, while a small spontaneous repolarization will reestablish resting potential V_r . Under these conditions, the active response is a *membrane action potential* as it occurs in an isolated cell or an uniformly polarized membrane. During membrane action potential, active ionic current is entirely transformed into capacitive current $i_{ion} = -i_c$ and electrotonic current $i_m = 0$ (Fig. 5). Only during the short time interval of extracellular current injection, electrotonic current $i_m = i_c + i_{ion} \neq 0$: the stimulus current is almost entirely used to charge the local cell membrane capacitor and none flows as local circuit current. Hence, during the stimulus, both i_c and i_{ion} flow outward with the same orientation: i_c has higher strength while i_{ion} is lower due to passive high resistance ion channels (Fig. 5). Once an action potential has been initiated by passing sufficient depolarizing current i_m to exceed threshold potential V_u , the stimulus current i_m may be set to zero.

In summary, the condition for excitation of a uniformly polarized membrane is that the voltage should reach and exceed a critical value V_u , the uniform threshold potential, corresponding to net ionic current $i_{ion} = 0$. In fact, net ionic current i_{ion} is outward for V_m within the interval $V_r < V_m < V_u$, zero for $V_m = V_u$ and inward for $V_m > V_u$ during the upstroke of the action potential (Figs. 4 and 5). It is worth noticing that during a membrane action potential i_{ion} , initially inward,

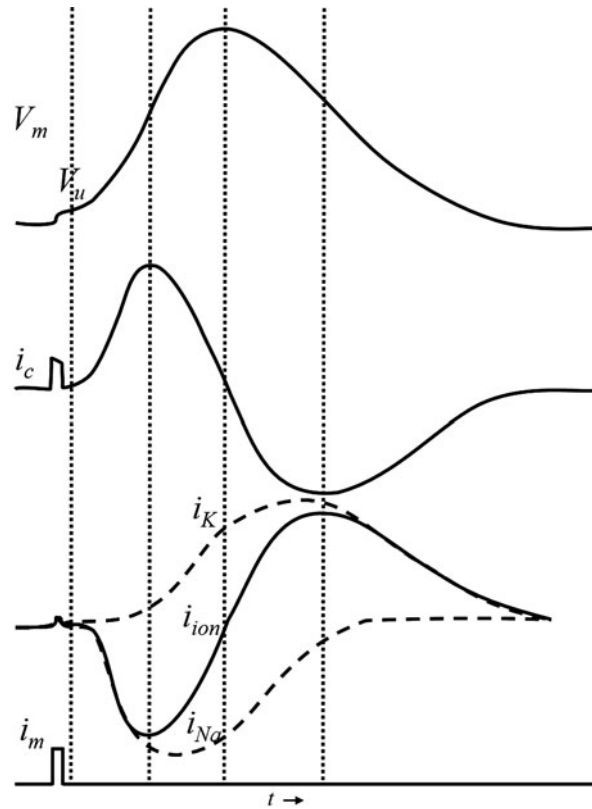


Fig. 5 Changes in voltage and currents during a membrane (uniform) action potential initiated by a brief rectangular stimulus current. The top diagram shows membrane potential change V_m as a function of time. The second diagram shows the capacity current $i_c = c_m dV_m/dt$. The initial, nearly square, wave corresponds to the applied current (see bottom diagram), most of which flows as capacity current when brief pulses are used. The third diagram shows the total ionic current (continuous curve) and its K^+ and Na^+ components (dashed curves). The bottom diagram shows the total membrane current $i_m = i_{ion} + i_c$, which is zero apart from time interval during which the stimulus is applied. The first dashed vertical line indicates when threshold V_u is reached while the following three dashed vertical lines indicate the times at which dV_m/dt is maximal, zero and minimal, respectively. This diagram may be compared with the corresponding one for a propagated action potential shown in Fig. 9. Adapted from Jack et al. [4]

reaches a minimum when dV_m/dt is maximal, is zero at the action potential peak when $dV_m/dt = 0$ and reaches a maximum when dV_m/dt is minimal.

Hence, when a uniform polarized membrane becomes an active source, i_{ion} entirely converts into i_c and the two currents flow in opposition, i.e. $i_{ion} = -i_c$.

5.2 The Propagating Action Potential

Conversely, when a cell is in contact with other cells as in cardiac tissue or long point-stimulated Purkinje fibers [2], active inward current i_{ion} generated by the cell membrane is not entirely transformed into i_c on the local membrane. Hence, $i_{ion} = -i_c + i_m$ and $i_m \neq 0$ is the electrotonic current that flows across cell membrane.

Let us consider a simple electrical model of an excitable cell as shown in Fig. 6 [4]. An external current pulse generator is connected to a model consisting of a resistor and capacitor in parallel. In addition, to represent the sodium current

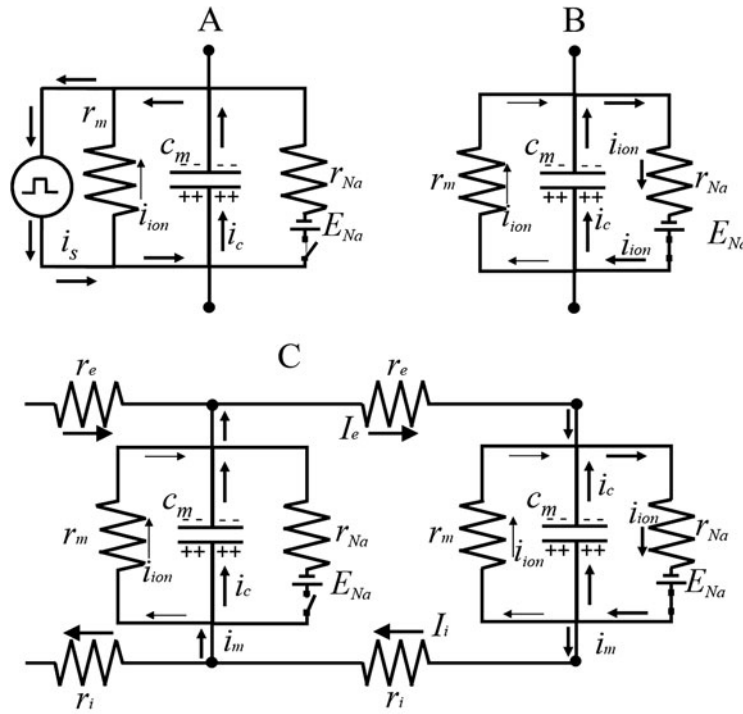


Fig. 6 Simple electrical circuits representing excitation and conduction. (a) an external current generator applies charge to the capacitance c_m of the model circuit. When the potential across the circuit reaches a threshold value, the switch on the Na^+ circuit closes and the Na^+ battery passes current into the cell. (b) the external current generator is removed. The potential change on the capacitance continues as current flows through the Na circuit and replaces the external current generator as the source of excitatory current. (c) the excited circuit is connected to a passive circuit and now acts like the external current generator in applying current to the passive circuit. Thus, the excitation may propagate for circuit to circuit. Since the Na^+ current in the excited circuit is the only inward current flowing, r_{Na} must be low (i.e. g_{Na} high) in order to allow sufficient Na^+ current to flow to continue charging the local capacitance and to excite the passive circuit. Hence there will be a minimal value of g_{Na} below which propagation cannot occur. Adapted from Jack et al. [4]

system, a battery E_{Na^+} (the Na^+ equilibrium potential) and resistance r_{Na^+} (the Na^+ active resistance) are also placed in parallel with the capacitor. A voltage-sensitive switch (i.e. the Na^+ channel ‘gates’), which closes when depolarization reaches Na^+ activation threshold, controls this circuit element. When a depolarizing current i_s is applied to the inside of the model (see *Intracellular current injection*), positive charge accumulates on the inside of the membrane capacitor (Fig. 6a). The potential changes in a positive direction and, therefore, a small outward current i_{ion} also flows across the passive high membrane resistance r_m . When Na^+ activation threshold is reached, the voltage dependent switch closes and an inward current is generated across the Na^+ resistance (Fig. 6b). It is assumed that the external impressed current pulse then terminates, i.e. the stimulating current is just threshold. This condition occurs when the charge furnished by the external impressed current pulse i_s (pulse strength · pulse duration) is turned off as soon as Na^+ activation threshold is reached. The inward flow of current across the Na^+ circuit now takes over the function of the external generator in applying positive charge to the inside of the membrane capacitance. Moreover, if this circuit were connected to a similar resting circuit, the current flowing across the sodium circuit could also apply positive charge to the capacitance of the resting circuit (Fig. 6c). The resting circuit would then also become excited and so a wave of excitation propagates from circuit to circuit. Such an arrangement of serially connected circuits can be used to represent the propagation process.

The condition for generating a propagating action potential in a cable is that the voltage at the point of current injection should exceed a critical value at which the net ionic current generated by the cable as a whole becomes inward. This critical voltage should be higher than V_u , the voltage threshold for excitation by uniform polarization. In order to determine the condition for exciting a cable by current applied at one point, it is useful to consider an expression for the i_{ion}/V_m relationship for the applied current I at a point $x = 0$ and the voltage V_m at the same point $x = 0$ (Fig. 7) as described by Jack et al. [4]. The equation derived by these authors is:

$$I = 2 \left(\frac{2}{r_i} \int_{V_r}^{V_m} i_{ion} dV \right)^{\frac{1}{2}}.$$

Since I becomes zero when the integral term is zero, the voltage threshold for cable excitation, expressed in terms of the voltage at the point of current injection, must be larger than the threshold for uniform membrane polarization V_u (Fig. 7). Moreover, provided that the $i_{ion}(V_m)$ relation is independent of time and the system is allowed to approach a steady-state before excitation occurs, the voltage threshold V_{Th} will be given by:

$$\int_{V_r}^{V_{Th}} i_{ion} dV = 0.$$

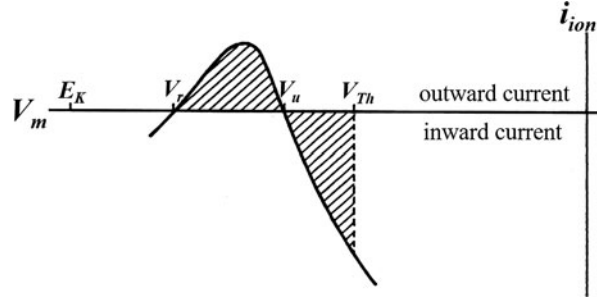


Fig. 7 Relation of voltage threshold for cable excitation V_{Th} to membrane current/voltage relation. V_r is the resting potential and V_u is the voltage threshold for excitation by uniform polarization. V_{Th} is given by the point at which the integral $\int_{V_r}^{V_{Th}} i_{ion} dV = 0$ becomes zero. Adapted from Jack et al. [4]

If there is no voltage that satisfy this equation, excitation cannot occur.

This equation may be more readily understood in terms of the corresponding curves for voltage V_m and current i_{ion} as function of distance x from the current source corresponding to threshold current applied at $x = 0$ (Fig. 8). The condition corresponding to the voltage threshold V_{Th} is that the integral of current with respect to distance should be zero so that no further current is required for the stimulation electrode, i.e.

$$\int_0^{\infty} i_{ion} dx = 0.$$

The length of fiber over which the excitation process occurs at threshold identifies the *liminal length* for excitation [5, 6]. The membrane region corresponding to the liminal length represents the *source*, delimited by V_{Th} where inward i_{ion} is maximal and by V_u , where i_{ion} is zero. The membrane region where i_{ion} is outward and V_m decreases exponentially to V_r represents the *sink*, i.e. the membrane region that has to be depolarized by intracellular current flowing from the source (Fig. 8).

An important question is how safe action potential propagation is under normal and pathological conditions. Shaw and Rudy [7] provided a comprehensive approach to the computation of the so-called safety factor (SF) using a multi-cellular theoretical fiber, as formulated by:

$$SF = \frac{\int_A i_c \cdot dt + \int_A i_m \cdot dt}{\int_A I_i \cdot dt}.$$

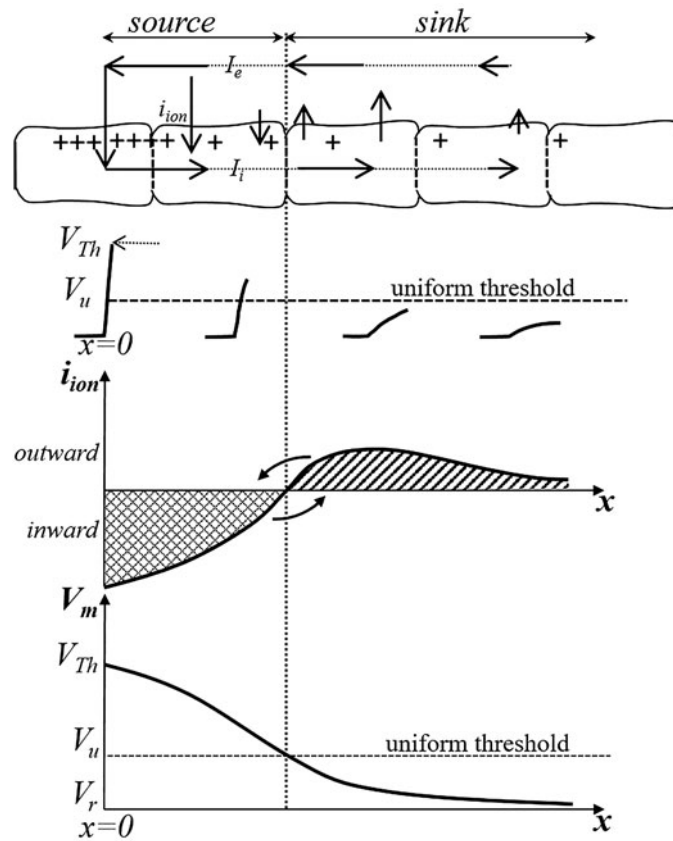


Fig. 8 Source, sink and liminal length. Upper panel: schematic diagram of currents flowing along a longitudinal sequence of cardiomyocytes induced by extracellular cathodal current injection at $x = 0$ reaching depolarization threshold. Ionic current i_{ion} , is inward in the source region where it is generated across the active membrane and outward in the sink region, i.e. electrotonic, across passive membrane that is being depolarized. Intracellular current I_i flowing from source to sink and extracellular current I_e flowing from sink to source complete the closed loop of current field lines. The source region identifies the liminal length comprised between threshold membrane potential for excitation V_{Th} at the point of current injection $x = 0$ and uniform threshold potential V_u at the point where sink region initiates. Middle panel: spatial variation in membrane current for threshold depolarization. Threshold is reached when the amount of inward current generated near the polarizing electrode is equal to the amount of (outward) repolarizing current generated by areas of membrane polarized below V_u . Lower panel: membrane potential V_m profile along source and sink, initiating at V_{Th} at the centre of the source and extending toward V_r , resting potential, where the sink ends. Adapted from Jack et al. [4]

The denominator of this equation corresponds to the electric charge flowing into a given cell during excitation and supplied by the neighboring active cell upstream (intracellular current I_i). The numerator represents the two terms into which the active ionic current i_{ion} generated by the cell divides. The first term refers to the

capacitive current i_c producing the upstroke of the action potential and the second term to the current i_m that transforms into I_i flowing out of the cell to excite neighboring resting cell downstream and to propagate the action potential. The integration range A relates to the time window during which the membrane is being depolarized, i.e. foot and upstroke of the action potential. Intuitively, this definition is straight-forward: propagation is safe if $SF > 1$, i.e. the denominator is smaller than the numerator, that is, if the electrotonic current required to excite a given cell (denominator) is smaller than the ionic current generated by this same cell (numerator). Hence, for a uniformly propagating action potential, the denominator of SF represents the threshold charge computed as time integral at a cell point, equivalent to the voltage integral of current at the point of current injection shown in Fig. 7 or the space integral of current with respect to liminal length shown in Fig. 8.

When excitation threshold is reached, action potential initiation and propagation occurs. The currents flowing during a propagated action potential are shown in Fig. 9. This figure represents an action potential propagating from right to left, initiating far away to the right, so that the action potential is already conducting as a wave of constant shape and speed. The first sign of arrival is an exponential rise in potential V_m , corresponding to the foot of the action potential. As indicated by the current diagram at the bottom of the figure, this phase corresponds to outward current flow i_m resulting from current flowing from the active region of membrane further to the right (source). During this phase, the source is acting as an external circuit applying depolarizing current i_m to the resting region ahead, the sink. The current flow i_m is almost entirely represented by i_c since the passive membrane conductance and ionic current i_{ion} are both very small.

Along action potential profile, the curve of ionic current i_{ion} is triphasic. At the foot of the action potential, ionic current i_{ion} is initially outward and, as sodium conductance increases, i_{ion} reaches a maximum and then declines to zero at V_u (Fig. 9, vertical line a) becoming inward. The membrane region where i_{ion} is outward and $V_r < V_m \leq V_u$ represents the sink. The inward flow of Na^+ current further depolarizes the membrane. Threshold potential V_{Th} is reached above V_u within interval $a-b$. In studies by Hoffman and Cranefield [8], SF associated with a propagated action potential in normal cardiac muscle was estimated to be more than six times that of diastolic threshold. As the Na^+ conductance inactivates and the K^+ conductance increases, the inward ionic current i_{ion} decreases. However, repolarization begins (Fig. 9, vertical line c) before the ionic current i_{ion} becomes outward (Fig. 9, vertical line a'). The reason for this is that, in addition to adding charge to the local membrane capacity, the inward flow of ionic current i_{ion} is also supplying local circuit current flow to regions of membrane that are already repolarizing. It continues to do so beyond the peak of the action potential, and for a period of time the local capacity and ionic currents flow in the same direction (interval $c-a'$). Ultimately, the ionic current i_{ion} vanishes and becomes outward (Fig. 9, beyond vertical line a') and the membrane potential returns towards its resting value.

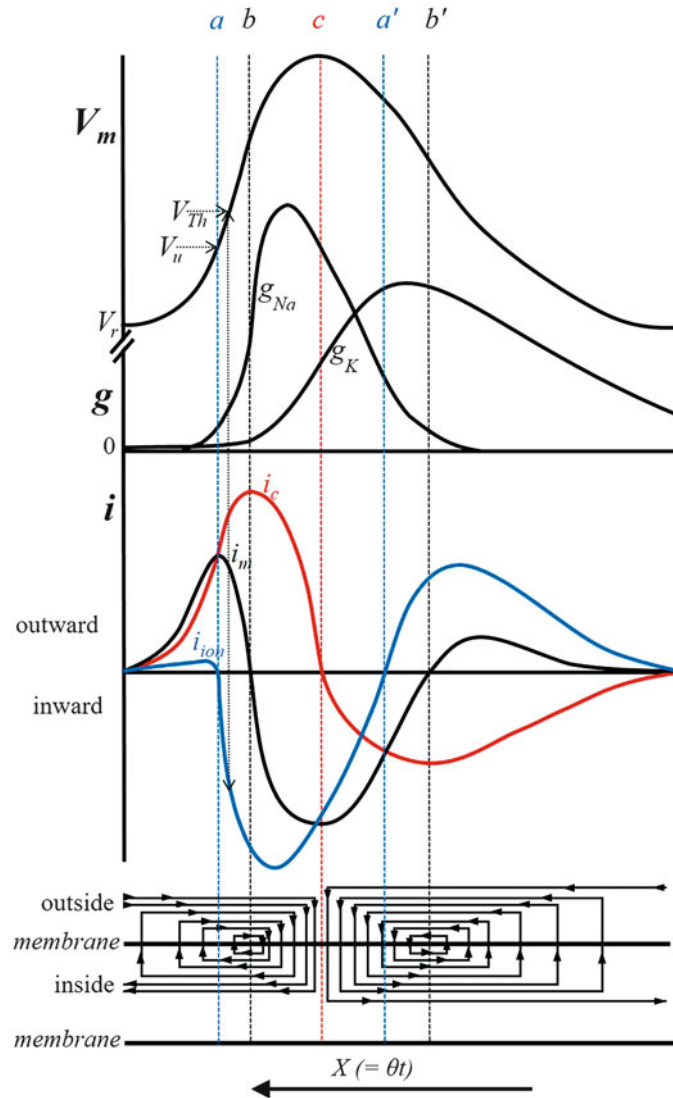


Fig. 9 The top curve shows membrane potential V_m . Immediately below are shown changes in g_{Na} and g_K conductances. The middle diagram shows the changes in i_m and its components, i_i and i_c . The bottom diagram is a schematic representation of the local circuits during propagation. The wave is propagating from right to left at uniform speed θ and the abscissa may also be regarded as time, since $x = \theta t$. The dashed vertical lines connect the points of the curves corresponding to zero crossing of i_{ion} , (line a and a'), zero crossing of i_m (line b and b') and zero crossing of i_c (line c). Note that (i) $i_m = 0$ for i_c at maximum and V_m at maximum depolarization rate (line a); (ii) $i_m = 0$ for i_c at minimum and V_m at maximum repolarization rate (line a'); (iii) $i_c = 0$ at V_m maximum value (peak of action potential). The source and sink regions are defined by the distances comprised between $V_r - V_u$ (outward i_{ion}) and $V_u - V_{Th}$ (inward i_{ion}), respectively. Adapted from Jack et al. [4]

Along action potential profile, the curve of membrane current i_m is also triphasic, being:

- outward along the foot and initial upstroke of the action potential and becoming zero at maximum depolarization rate (Fig. 9, vertical line b , maximum of i_c curve);
- inward within interval $b-b'$ in Fig. 9, reaching a minimum at peak of action potential (Fig. 9, vertical line c , $i_c = 0$) and becoming zero at maximum repolarization rate (Fig. 9, vertical line b' , minimum of i_c curve);
- outward beyond vertical line b' in Fig. 9, where $i_m = 0$.

Interestingly, the current curves shown in this figure may all be obtained experimentally from measurements of the propagating action potential [9]. The capacity current i_c is obtained by differentiating the action potential,

$$i_c = C_m \frac{\partial V_m}{\partial t}.$$

Moreover, transmembrane current i_m may be obtained from the second derivative since, when the wave conducts with a constant shape and velocity, the time and distance scale are proportional, the constant of proportionality being θ , the conduction velocity. Hence, transmembrane current i_m becomes:

$$i_m = \frac{1}{r_i \theta^2} \frac{\partial^2 V_m}{\partial t^2}.$$

The ionic current i_{ion} may then be computed as the difference between i_m and i_c .

In summary, inward current i_m flowing across active membrane undergoing rapid depolarization and early repolarization gives rise to axial current I_i flowing in opposite directions along fiber axis. Partition point for i_m occurs at the peak of action potential profile. Axial current I_i transforms into outward electrotonic current, mainly capacitive, that sustains propagation ahead of action potential profile and delays repolarization phase behind. Hence, the amount of electrotonic current flowing behind direction of propagation modulates action potential profile, i.e. action potential duration (APD).

6 Electrotonic Modulation of Repolarization by the Activation Sequence

As compared to a cable like structure where action potential propagation is one-dimensional, propagation in cardiac muscle is three-dimensional. Electrotonic modulation of repolarization is more complex than the classic electrotonus described by cable theory for strands or axons with constant values of membrane resistance and uniformly distributed longitudinal resistance. It is well known that spatial dispersion

of repolarization plays an important role in arrhythmogenesis. At tissue level, intrinsic APD heterogeneity can be modulated by electrotonic interactions between cells [10]. Regional variations of APD represent a form of electrophysiological heterogeneity in the heart. In a wide range of species, spatial gradients of APD exist from base to apex, from right to left ventricle and in the transmural plane of healthy myocardium [11, 12]. Furthermore, electrotonic interactions during repolarization can lead to dynamic modulation of APD gradients depending on the activation sequence, leading to an inverse linear relationship between activation time (AT) and APD [10, 13–20]. The dynamic nature of this modulation is due, in part, to the spatial gradient in membrane potential occurring during the repolarization phase of a propagating AP. Each cell is influenced by the electrotonic load from its neighbors such that, cells repolarizing later generate an inward electrotonic current flowing toward their earlier repolarizing neighbors with the effect of delaying repolarization phase. In homogeneous tissue, electrotonic modulation of repolarization effectively prolongs the APD of the earlier activated cells and generates gradually decreasing APDs away from the pacing site. These APD gradients are most pronounced at the pacing site, at the tissue boundaries and in directions of slow propagation [18, 21, 22].

6.1 Modulation of Activation-Recovery Interval

Experimental evidence of acute electrotonic modulation of repolarization during two different activation sequences, sinus rhythm (SR) and ventricular drive (VD), can be obtained by electrical mapping in the in situ heart. An unpublished experimental result from our laboratory is shown in Fig. 10. Unipolar potential mapping was performed from the anterior ventricular surface in rat heart by means of an 8×8 epicardial electrode array, with 1-mm resolution square mesh [23]. Unipolar stimulation at a ventricular test site was obtained from one of the array electrodes by means of 1 ms duration and twice diastolic-threshold strength cathodal current pulses. Ventricular ATs were computed from unipolar epicardial electrograms as the times of the minimum time derivative (dV/dt_{\min}) during QRS complex and referenced to QRS or stimulus onset for SR and ventricular drive, respectively. Recovery times (RT) were computed as the times of the minimum of the time derivative (dV/dt_{\min}) during the downslope of the T wave. Activation recovery interval (ARI), a well-validated estimate of local APD [24, 25] was obtained as difference between AT and RT. Isochrone line maps in Fig. 10 display the general time course and spatial distribution of AT, RT and ARI on the anterior ventricular epicardium during normal SR and VD at a test site located on the anterior paraseptal area.

Commonly, during normal SR in rat heart [26, 27] two breakthrough points (BTPs) characterize ventricular activation onset on the lateral right (RV) and left (LV) ventricular surfaces, respectively (not shown because outside the electrode array). Thereafter, two planar wave fronts that originate from the two BTPs prop-

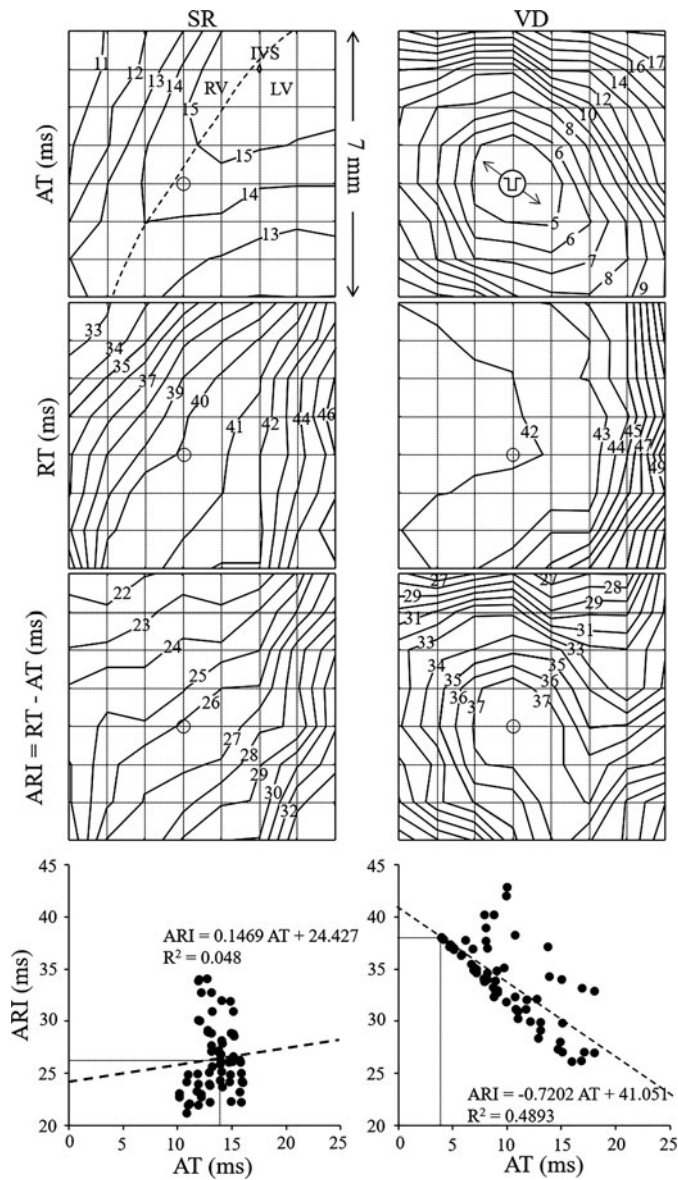


Fig. 10 Isochrone line maps during sinus rhythm (SR) and ventricular drive (VD) computed from electrograms recorded by a 8×8 epicardial electrode array in rat heart. AT, activation times; RT, repolarization times; ARI = RT - AT, activation recovery intervals; current pulse symbol, pacing site; circle, electrode corresponding to pacing site; double headed arrow, fiber direction at pacing site; RV, right ventricle; LV, left ventricle; IVS, interventricular septum. AT and RT isochrone numbers, milliseconds from QRS or stimulus onset during SR or VD, respectively. Bottom diagram: relationships between AT and ARI displayed by linear regression analysis at each array electrode. A good linear relationship occurs at points around pacing site. Correlation coefficient R^2 for VD is reduced by the presence of ARI at electrodes distant from pacing site, at lower right and left corners of the electrode array

agate from RV and LV along epicardial fiber direction toward the interventricular septum (IVS) (Fig. 10, SR, AT). The two wave fronts collide over the IVS and merge into a new V-shaped wave front that spreads toward the RV outflow tract, mainly across epicardial fiber direction.

RTs display uniform spatial dispersion on the anterior epicardial surface (Fig. 10, SR, RT). In particular, on the RV, recovery isochrones mainly follow the activation sequence toward the IVS with uniform parallel lines. The density of recovery isochrones is higher toward the paraseptal area indicating a pronounced recovery gradient oriented perpendicularly to the IVS. On the LV, recovery isochrones propagate away from the IVS with uniform parallel lines toward LV free wall.

ARI isochrones display uniform spatial dispersion oriented from RV to LV, similarly to RT isochrones (Fig. 10, SR, ARI).

Conversely, activation isochrones during ventricular drive were elongated, symmetric, and quasi-elliptical around the pacing site with the major axis oriented along the local sub-epicardial fiber direction (Fig. 10, VD, AT). Recovery isochrones show that onset of repolarization occurs at pacing site and that RTs are almost constant up to a distance of few λ (2–3 mm) [3] around pacing site. The different spatial distribution of RTs during VD compared to SR is due to the different electrotonic modulation of repolarization by the two activation sequences at test site: symmetric during VD compared to planar during SR.

ARI spatial distribution during VD is heterogeneous, with the longest duration at pacing site that gradually decreases with distance in all directions: longest ARI (37 ms) is observed at pacing site and shortest ARI (27 ms) lays close to the site of the latest AT (Fig. 10, VD, ARI).

The relationship between AT and ARI at each array electrode is displayed by linear regression analysis. A clear decreasing trend of ARI with AT is revealed during VD (slope = -0.72): electrode sites activating earliest have longer ARIs and electrode sites activating later have shorter ARIs. Similar negative correlation between AT and either ARI or APD has previously been reported in experimental models [18, 28] and humans [16]. A likely mechanism for the relationship is local electrotonic current flow between cells which tends to equalize action potential durations. This coupled with the later repolarization of cells downstream and electrotonic current flow from cells downstream to cells upstream would contribute to the AT–ARI gradient [29]. Conversely, during SR a relatively shallow relationship and an undefined correlation links ATs and ARIs.

Hence, at an electrode site, different ARI values and, correspondingly, different APDs are present, depending on the activation sequence. In particular, Fig. 10, shows that at an electrode site ARI is shorter during SR (26 ms) than during VD at the same site (38 ms). Hence, different APD values can be measured at a myocardial site depending on the different activation sequence occurring at that site, likely due to the different electrotonic modulation of repolarization. It is known that dispersion of RT is an important determinant of the vulnerability to arrhythmias following a premature activation. However, in our experiments we found that, due to electrotonic interactions, RT spatial distribution in the normal rat heart was uniform during SR and relatively homogeneous during VD. These results suggest that normal

ventricular myocardium would be resistant against arrhythmias following ectopic activation, at least in the rat heart.

6.2 *Modulation of Effective Refractory Period*

In experimental and clinical electrophysiology studies, refractoriness is measured by the effective refractory period (ERP). In normal myocardium, there is a close temporal relationship between ERP and APD, and the two are often used as estimates of each other, although this relationship is altered in ischemic myocardium where the recovery of excitability lags behind full repolarization (postrepolarization refractoriness).

ERP can be measured as the interval from depolarization to the recovery of excitability when stimulation fails to induce a propagated response. The classic technique for ERP measurement is the extra-stimulus technique where a train of eight basic stimuli S1 is followed by a single premature stimulus S2 elicited at the same site (test site drive). Alternatively, ERP duration can also be measured by the extra-stimulus technique during SR, which consists of a sequence of eight sinus beats (RW, the upward deflection of the QRS complex) followed by a single premature stimulus (S). Unpublished experimental findings in rat heart show that ERP durations measured by the two protocols, S1–S2 and RW-S, are different and consistent with the difference in ARI values measured during corresponding sequences of basal ventricular activation, i.e. VD and SR. In fact, ERP is shorter when measured during RW-S than during S1–S2. Interestingly, at the same site, ERP difference is the same as ARI difference. Hence, it is hypothesized that also ERP difference is likely due to the different electrotonic modulation of repolarization by the different activation sequence. Consequently, different APDs measured at an electrode site during SR and VD would also imply correspondingly different ERPs measured at the same site. Experimental verification of electrotonic modulation of ERP by the activation sequence is shown in Fig. 11 where ERP measured at a test site during VD (S1–S2 protocol) and SR (RW-S protocol) was 90 ms and 72 ms, respectively.

Since APD changes are also function of rate, with the APD at steady-state shorter the higher the frequency, it can be argued that the different ARI (or APD) measured values are due to the different basal ventricular activation rates (S1 and SR). However, in contrast to this argument, ARI values are longer during S1 drive at a frequency higher than SR. Moreover, the difference between ARI and ERP values did not change when SR rate was matched to that of S1 drive by means of atrial drive (AD) (Fig. 11). Hence, it can be concluded that, at least for frequencies used in our experiments, electrotonic modulation of repolarization by the activation sequence is responsible for dynamic modulation of ARI and ERP gradients.

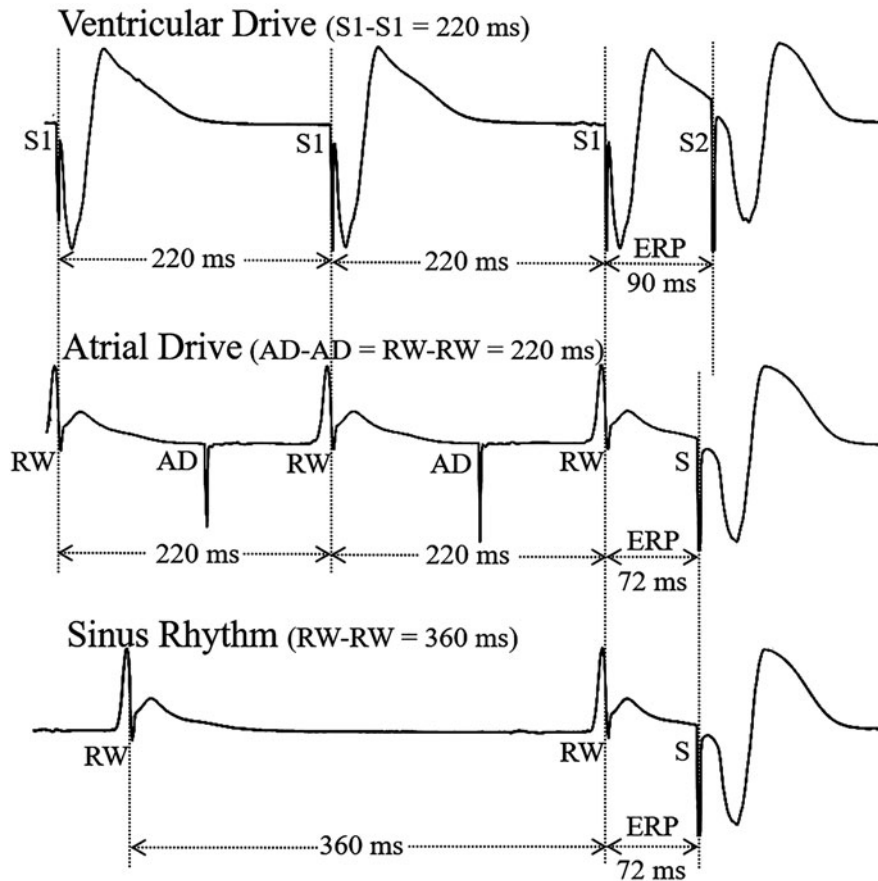


Fig. 11 Reference electrogram displaying pacing protocols for effective refractory period (ERP) measurement by premature stimulation (S2 or S) during Ventricular Drive (S1-S1), Atrial Drive (AD-AD) and Sinus Rhythm (RW-RW). Results show that ERP is longer when measured during S1-S2 than RW-S protocol, irrespective of S1-S1 or RW-RW cycle length. See text for explanation

7 Summary and General Conclusions

In summary, electrotonic current is a transmembrane current, provided by either an external current generator or an active region of cell membrane, which depolarizes membrane potential locally.

In case of an external current generator, the stimulating extracellular electrode (cathode) removes current I_e from the surrounding extracellular volume including outward transmembrane current i_m from excitable tissue. The stimulating current $i_m = i_c + i_{ion}$ depolarizes membrane potential V_m by means of capacitive component i_c that forces ionic component i_{ion} to flow across passive membrane resistance r_m .

Both i_c and i_{ion} are outward currents that flow with the same orientation across the membrane. On reaching excitation threshold at the stimulation site, action potential initiation and propagation occurs from the stimulating electrode with opposite orientation along cell axis.

In case of an active membrane region, as it occurs for a propagating action potential, the membrane itself is a current source generating inward ionic current i_{ion} whose largest fraction turns into outward capacitive current i_c depolarizing source membrane potential. It is worth noting that i_{ion} and i_c flow with opposite orientation across the active membrane region. The fraction of i_{ion} that is not used to depolarize membrane potential as i_c at the source region, i.e. $i_m = i_{ion} + i_c$, flows into the cell transforming into intracellular current I_i . Current I_i flows from the source region in opposite orientation sustained by V_m potential gradients along cell axis. The inversion point for the opposite flow occurs at the peak of the action potential profile. I_i flows downstream towards the sink region, down the slope of action potential upstroke. In the sink region, I_i transforms into transmembrane current $i_m = -\frac{\partial I_i}{\partial x} = \frac{\partial I_e}{\partial x} = i_c + i_{ion}$ that depolarizes membrane potential to threshold by means of i_c greater than i_{ion} , due to high r_m value. I_i flows upstream from the source region along the repolarization slope of action potential profile transforming into outward depolarizing i_m that delays repolarization phase and prolongs APD.

A clear definition of electrotonic current and its mechanism of action is of particular importance in cardiac electrophysiology, where APD heterogeneity is in part determined by the intrinsic properties of the myocardial cells, but it has also been shown to depend on cell-to-cell coupling and activation patterns [18]. Electrotonic interactions due to the coupling of cells in tissue are capable of gradually decreasing the duration of an action potential as it propagates away from the pacing site, with the strongest effect found in the direction of small conduction velocities or for reduced coupling. Cell-to-cell coupling has also been found to modulate the rate-dependency of APD, i.e. APD restitution [30]. Since the steepness of APD restitution has been implicated in arrhythmogenesis, it is important to understand which factors can modulate this dynamical property of cardiac tissue. Epicardial potential measurements in a rat experimental model, suggest that APD is shorter at later activation times independent on basal pacing frequency. However, these findings require validation for a broad range of basal pacing frequencies.

References

1. Plonsey, R., Barr, R.C.: Bioelectricity. A Quantitative Approach, 3rd edn. Springer, Heidelberg (2007)
2. Fozzard, H.A., Schoenberg, M.: Strength-duration curves in cardiac Purkinje fibres: effects of liminal length and charge distribution. *J. Physiol.* **226**, 593–618 (1972)
3. Weidmann, S.: Electrical constants of trabecular muscle from mammalian heart. *J. Physiol.* **210**, 1041–1054 (1970)
4. Jack, J.J.B., Noble, D., Tsien, R.W.: Electric Current Flow in Excitable Cells. Clarendon Press, Oxford (1975)

5. Rushton, W.A.H.: Initiation of the propagated disturbance. *Proc. R. Soc. B.* **124**, 210–243 (1937)
6. Noble, D.: The relation of Rushton's 'liminal length' for excitation to the resting and active conductances of excitable cells. *J. Physiol.* **226**, 573–591 (1972)
7. Shaw, R.M., Rudy, Y.: Ionic mechanisms of propagation in cardiac tissue. Roles of the sodium and L-type calcium currents during reduced excitability and decreased gap junction coupling. *Circ. Res.* **81**, 727–741 (1997)
8. Hoffman, B.F., Cranefield, P.F.: *Electrophysiology of the Heart*. McGraw Hill, New York (1960)
9. Cole, K.S., Curtis, H.J.: Electric impedance of the squid giant axon during activity. *J. Gen. Physiol.* **22**, 649–670 (1939)
10. Laurita, K.R., Girouard, S.D., Rudy, Y., Rosenbaum, D.S.: Role of passive electrical properties during action potential restitution in intact heart. *Am. J. Phys.* **273**, H1205–H1214 (1997)
11. Antzelevitch, C.: Modulation of transmural repolarization. *Ann. N. Y. Acad. Sci.* **1047**, 314–323 (2005)
12. Wan, X., Bryant, S.M., Hart, G.: The effects of $[K^+]_o$ on regional differences in electrical characteristics of ventricular myocytes in guinea pig. *Exp. Physiol.* **85**, 769–774 (2000)
13. Banville, I., Gray, R.A.: Effect of action potential duration and conduction velocity restitution and their spatial dispersion on alternans and the stability of arrhythmias. *J. Cardiovasc. Electrophysiol.* **13**, 1141–1149 (2002)
14. Chauhan, V.S., Downar, E., Nanthakumar, K., Parker, J.D., Ross, H.J., Chan, W., Picton, P.: Increased ventricular repolarization heterogeneity in patients with ventricular arrhythmia vulnerability and cardiomyopathy: a human in vivo study. *Am. J. Physiol. Heart Circ. Physiol.* **290**, H79–H86 (2006)
15. Franz, M.R., Bargheer, K., Rafflenbeul, W., Haverich, A., Lichtlen, P.R.: Monophasic action potential mapping in human subjects with normal electrocardiograms: direct evidence for the genesis of the T wave. *Circulation.* **75**, 379–386 (1987)
16. Hanson, B., Sutton, P., Elameri, N., Gray, M., Critchley, H., Gill, J.S., Taggart, P.: Interaction of activation-repolarization coupling and restitution properties in humans. *Circ. Arrhythm. Electrophysiol.* **2**, 162–170 (2009)
17. Myles, R.C., Bernus, O., Burton, F.L., Cobbe, S.M., Smith, G.L.: Effect of activation sequence on transmural patterns of repolarization and action potential duration in rabbit ventricular myocardium. *Am. J. Physiol. Heart Circ. Physiol.* **299**, H1812–H1822 (2010)
18. Walton, R.D., Benson, A.P., Hardy, M.E., White, E., Bernus, O.: Electrophysiological and structural determinants of electrotonic modulation of repolarization by the activation sequence. *Front. Physiol.* **4**, 281 (2013)
19. Yuan, S., Kongstad, O., Hertervig, E., Holm, M., Grins, E., Olsson, B.: Global repolarization sequence of the ventricular endocardium: monophasic action potential mapping in swine and humans. *Pacing Clin. Electrophysiol.* **24**, 1479–1488 (2001)
20. Yue, A.M., Betts, T.R., Roberts, P.R., Morgan, J.M.: Global dynamic coupling of activation and repolarization in the human ventricle. *Circulation.* **112**, 2592–2601 (2005)
21. Joyner, R.W.: Modulation of repolarization by electrotonic interactions. *Jpn. Heart J.* **27**(Suppl 1), 167–183 (1986)
22. Zubair, I., Pollard, A.E., Spitzer, K.W., Burgess, M.J.: Effects of activation sequence on the spatial distribution of repolarization properties. *J. Electrocardiol.* **27**, 115–127 (1994)
23. Rossi, S., Buccarello, A., Ershler, P.R., Lux, R. L., Callegari, S., Corradi, D., Carnevali, L., Sgoifo, A., Miragoli, M., Musso, E., Macchi, E.: Effect of anisotropy on ventricular vulnerability to unidirectional block and reentry by single premature stimulation during normal sinus rhythm in rat heart. *Am. J. Physiol. Heart Circ. Physiol.* **312**, H584–H607 (2017)
24. Haws, C.W., Lux, R.L.: Correlation between in vivo transmembrane action potential durations and activation-recovery intervals from electrograms. Effects of interventions that alter repolarization time. *Circulation.* **81**, 281–288 (1990)

25. Millar, C.K., Kralios, F.A., Lux, R.L.: Correlation between refractory periods and activation-recovery intervals from electrograms: effects of rate and adrenergic interventions. *Circulation*. **72**, 1372–1379 (1985)
26. Macchi, E., Cavalieri, M., Stilli, D., Musso, E., Baruffi, S., Olivetti, G., Ershler, P.R., Lux, R.L., Taccardi, B.: High-density epicardial mapping during current injection and ventricular activation in rat hearts. *Am. J. Physiol. Heart Circ. Physiol.* **275**, H1886–H1897 (1998)
27. Rossi, S., Baruffi, S., Bertuzzi, A., Miragoli, M., Corradi, D., Maestri, R., Alinovi, R., Mutti, A., Musso, E., Sgoifo, A., Brisinda, D., Fenici, R., Macchi, E.: Ventricular activation is impaired in aged rat hearts. *Am. J. Physiol. Heart Circ. Physiol.* **295**, H2336–H2347 (2008)
28. Burgess, M.J., Steinhaus, B.M., Spitzer, K.W., Green, L.S.: Effects of activation sequence on ventricular refractory periods of ischemic canine myocardium. *J. Electrocardiol.* **18**, 323–329 (1985)
29. Toyoshima, H., Burgess, M.: Electrotonic interaction during canine ventricular repolarization. *Circ. Res.* **43**, 348–356 (1978)
30. Qu, Z.: Dynamical effects of diffusive cell coupling on cardiac excitation and propagation: a simulation study. *Am. J. Physiol. Heart Circ. Physiol.* **287**, H2803–H2812 (2004)

Emilio Macchi graduated with a master's in physics, Università degli Studi, Milano, in 1969. He obtained a PhD in 1973 from the Department of Physiology and Biophysics, Dalhousie University, Halifax, Nova Scotia, Canada, under the supervision of Prof. Pentti M. Rautaharju. Subsequently, he became research associate at the Istituto di Cardiologia Sperimentale, Simes-SPA, Milano, in the Electrophysiological Laboratory of Professor Bruno Taccardi (1974–1976); Full-time Researcher at the Istituto per le Applicazioni del Calcolo “Mauro Picone,” National Research Council, Rome (1976–1987); Associate Professor of General Physiology, Istituto di Fisiologia Generale, Università degli Studi, Parma (1987–1994); and Professor of Physiology, Dipartimento di Biologia Evolutiva e Funzionale and Dipartimento di Bioscienze, Università degli Studi, Parma (1994–2016). He is now Professor Emeritus at the Dipartimento di Scienze Chimiche, della Vita e della Sostenibilità Ambientale, Università di Parma. Dr. Macchi has been Visiting Professor at the Cardiovascular Research and Training Institute, University of Utah, Salt Lake City, USA, during different periods in 1986–1989. He also served as Director of the Dipartimento di Biologia Evolutiva e Funzionale, Università degli Studi, Parma (2004–2008).

Dr. Macchi's scientific activity is documented by 75 full articles/reviews/chapters in books and relates to measurement and modeling of the cardiac electric field in mathematical and animal models and in man. Independent research work in cardiac electrophysiology continuously progressed in collaboration with Prof. Bruno Taccardi and Prof. Ezio Musso. Relevant results of these studies were relationship between extracellular potential distribution and intra-cardiac electric sources, identification of the oblique dipole layer model of the activation wave front as a realistic equivalent generator presently utilized in experimental and clinical electrophysiology studies, definition of an olive-shaped intra-cavitary probe for arrhythmia detection in experimental, and clinical electrophysiology studies.

Ezio Musso completed his university studies at the University of Pavia (Italy) where he obtained the MD degree (1965) and specialization in cardiology (1971). In 1966, he started his research activity in the Electrophysiological Laboratory of Professor Bruno Taccardi in Milano. Subsequently, he became Assistant Professor of Physiology at the University of Parma, Italy (1974–1980) and Full Professor of Physiology at the same university (1980–2011) where he also served as Director of the Institute of General Physiology and/or the Department of Evolutionary and Functional Biology (1987–2011). He was Visiting Scientist/Visiting Assistant Professor of Physiology/Visiting Professor of Medicine at Laboratoires de Physiologie Comparée et de Physiologie Cellulaire associé au CNRS, Faculté de Sciences, Orsay-Paris (1969); Department of Physiology, State University of New York, Downstate Medical Center, Brooklyn-New York (1972–1975, 1976, 1977, 1981); and Cardiovascular Research Institute, New York Medical College, Valhalla-New York (2002–2004; 2005; 2006).

Dr. Musso's research in cardiac electrophysiology has focused on autonomic control of cardiac automatism, biophysical aspects and clinical applications of the cardiac electric field mechanisms of onset of arrhythmias, cardiovascular response to stress, stem cell-mediated cardiac regeneration, and mechanical and electrical competence of the regenerated heart.

His scientific activity is documented by more than 150 papers "in extenso" (the largest part of which has been published in the most reputable scientific journals) and chapters in books. His work has been funded with national, European, and NIH grants.

Stefano Rossi is assistant researcher at the Department of Medicine and Surgery, University of Parma. In 2006, he obtained a PhD in "Systemic Pathophysiology" at the Department of Evolutionary and Functional Biology, University of Parma. He was winner of a 4-year research grant for the study of cardiac electrical activity in elderly rats and a 3-year research grant for the study of atmospheric particulate effects on arrhythmogenesis in normotensive and hypertensive rats. He is also a collaborator of several research projects concerning the study of cardiac electrophysiological properties through electric epicardial mapping on different experimental models such as ischemic rats treated with cardiac stem cells, dystrophic mice, stressed rats, and hypertensive rats. Dr. Rossi is the author of 26 scientific publications in international journals with impact factor and reviewer for several international journals in the field of cardiac electrophysiology. Currently, he is involved in the study of arrhythmogenesis in normal cardiac tissue and nanotoxicity effects within the cardiovascular system.